JOURNAL OF GEOPHYSICAL RESEARCH: OCEANS, VOL. 118, 856–868, doi:10.1002/jgrc.20070, 2013

Generation of an estuarine sediment plume by a tropical storm

Peng Cheng,[1] Ming Li,[1] and Yun Li[1]

Received 21 May 2012; revised 3 December 2012; accepted 20 December 2012; published 20 February 2013.

[1] Tropical Storm Lee (2011) caused a record flood in the Susquehanna River which discharged about 6.7 million tons of suspended sediments into the Bay, an amount equal to the input of 6 average years. The flood-carried sediment produced a large sediment plume that covered one half of Chesapeake Bay with the maximum suspended sediment concentration exceeding 2500 mg L^{-1}. Three stages were identified in the development of the sediment plume, corresponding to three dominant forcing mechanisms, i.e., river flow, estuarine circulation, and sediment settling. Most of the flood-carried sediments were deposited in the Bay within 20 days. Sands were dumped in the Susquehanna Flats with a maximum thickness of 10 cm, while fine-grained sediments were dusted over a wide area in the upper Bay with a maximum thickness of 4 cm. Long-term simulation of the post-storm period showed that a majority of the flood sediments were redistributed to accumulate in the estuarine turbidity maximum region due to flood–ebb asymmetry in tidal suspension and advection by estuarine circulation and tidal flows while the rest were transported seaward and deposited in the mid-Bay. It is estimated that the flood delivered 9 months of particulate nitrogen and over 1 year of particulate phosphorus supplies to the estuary. This catastrophic event may change the geological history and exacerbate water-quality decline in the American largest estuary.

Citation: Cheng, P., M. Li, and Y. Li (2013), Generation of an estuarine sediment plume by a tropical storm, *J. Geophys. Res. Oceans*, *118*, 856–868, doi:10.1002/jgrc.20070.

1. Introduction

[2] The U.S. East and Gulf Coasts have experienced elevated tropical storm and hurricane activity in recent years, a pattern that is expected to persist for several more decades and may increase due to global warming [*Goldenberg et al.*, 2001; *Emanuel*, 2005; *Webster et al.*, 2005]. These extreme weather events not only can produce storm surges and heavy rainfall causing coastal inundations but also may discharge massive amounts of nutrients, suspended sediments, and organic materials into coastal oceans [*Geyer et al.*, 2000; *Harris et al.*, 2005; *Gong and Shen*, 2009]. The floods induced by extreme precipitation often deposit huge amounts of sediment in short time periods, comprising the majority of the stratigraphic record in many settings [*Wheatcroft and Borgeld*, 2000]. Studies of sediment transport on continental shelves have recognized the importance of oceanic flood sedimentation in coastal environments [*Sommerfield and Nittrouer*, 1999; *Wheatcroft*, 2000] and revealed that fluid-mud flows during oceanic floods play a crucial role in cross-shelf sediment escaping [*Traykovski et al.*, 2000; *Ogston et al.*, 2000; *Wright et al.*, 2001] and the formation of strata [*Wheatcroft and Borgeld*, 2000; *Mullenbach and Nittrouer*, 2000].

[3] Estuaries, the main conduit between rivers and ocean, act as a filter for river-borne sediment. It has been estimated that over 90% of sediments reaching the East Coast of the United States are trapped within estuaries [*Meade*, 1982]. This trapping function makes estuaries particularly vulnerable to heavy sediment discharge and its associated delivery of nutrients and contaminants. In the history of Chesapeake Bay, the passage of Tropical Storm Agnes in June of 1972 has been widely considered as a catastrophic event that remodeled Chesapeake Bay and may have contributed to the initiation of long-term water-quality decline in the American largest estuary. Agnes brought record rainfall to the drainage basins of Chesapeake Bay's tributaries, and resulted in a 1-in-200 flood in the Susquehanna River with the maximum daily discharge reaching 32,000 m^3 s^{-1} [*Page and Shaw*, 1973]. In the 10 day period, the flood of Agnes discharged about 31 million tons of suspended sediment into the northern Chesapeake Bay, an amount equivalent to the input of 30 average years [*Schubel*, 1977]. It also overloaded the Bay with nutrients and organic matters that led to elevated plankton production for several years [*Loftus and Seliger*, 1976]. The sediment discharge disrupted entire biological community to some degree. In particular, submerged aquatic plants decreased 67%, and eelgrass decreased 89% [*Kerwin et al.*, 1976]. In the tributaries to the lower Bay, eelgrass did not recover to the pre-Agnes level through 2004 [*Lynch*, 2005].

[4] Tropical Storm Lee (TS Lee hereafter) made landfall in Louisiana on 4 September 2011 and moved across the Middle Atlantic Region on 7–10 September. With weak winds and heavy precipitation, it exhibited remarkable similarity to Tropical Storm Agnes (Figure 1). Since the winds were weak, TS Lee did not produce large storm surges in

[1]Horn Point Lab, University of Maryland Center for Environmental Science, Cambridge, Maryland, USA.

Corresponding author: M. Li, Horn Point Lab., University of Maryland Center for Environmental Science, 2020 Horn Point Road, Cambridge, MD 21613, USA. (mingli@umces.edu)

2169-9275/13/10.1002/jgrc.20070

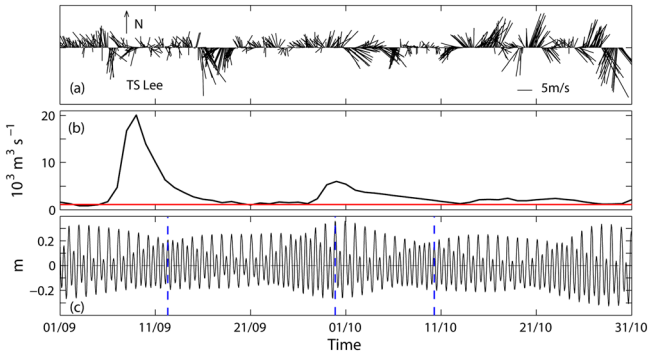

Figure 1. (a) Wind speed vector at the Patuxent River Naval Air station (see Figure 3 for its location). (b) Discharge of the Susquehanna River at the USGS station in Conowingo, Maryland. The peak discharge is about 18 times of the annual mean discharge (shown as the red line). (c) Surface water elevation at NOAA tidal observation station Tolchester beach (see Figure 3 for its location). The three blue dashed lines indicate times selected for the analysis of the sediment transport equation in Figures 11 and 12.

Figure 2. Satellite true color image of the Chesapeake Bay region on 13 September 2011. A large sediment plume covered over one half of Chesapeake Bay (Courtesy of NASA).

the Bay. However, the torrential rain from the remnants of TS Lee caused the second largest record flood in the Susquehanna River: the peak river discharge reached 22,031 m^3/s (18 times of the annual average) at the U.S. Geological Survey (USGS) stream site Conowingo, Maryland on 9 September (Figure 1b). According to the curve of recurrence interval of peak river flow at Conowingo [*Page and Shaw*, 1973], the flood has a recurrence interval of 90 years. The storm washed a massive amount of sediments into Chesapeake Bay, producing a large brown sediment plume, as captured in satellite images (Figure 2, see mddnr.chesapeakebay.net for more images). The deluge-carried sediment could significantly impact the sedimentary history and ecosystem productivity of Chesapeake Bay.

[5] TS Lee provides a rare opportunity to study the effects of tropical storms on estuarine systems. In this study, we use a coupled hydrodynamic-sediment transport model to investigate the sediment plume generated by the storm and map out deposition pattern of fluvial sediment on the seabed. Specific objectives are to: (1) estimate the total sediment input from the Susquehanna River to the Bay, (2) investigate the sediment dispersion processes, (3) quantify the deposition of the fluvial sediment, and (4) explore the effects of the fluvial sediment on the ecosystem of Chesapeake Bay.

2. Numerical Model

2.1. Model Configuration

[6] A 3D hydrodynamic model of Chesapeake Bay based on ROMS [*Haidvogel et al.*, 2000] has been developed (Figure 3) and validated against observations [*Li et al.*, 2005, 2006; *Zhong and Li*, 2006]. We used a finer-resolution version of this model to simulate the Bay's response to TS Lee. The model has 240×160 horizontal grids and 20 vertical layers. The model is forced by freshwater inflows at river heads, tidal, and nontidal flows at the offshore boundary, and winds and heat exchanges across the water surface. The open-ocean boundary condition consists of Chapman's condition for surface elevation, Flather's condition for barotropic velocity, and Orlanski-type radiation condition for baroclinic velocity. At the upstream boundary in the eight major tributaries, freshwater inflows obtained at USGS gauging stations are prescribed. At the offshore open boundary, we apply a combination of Orlanski-type radiation condition and nudging [*Marchesiello et al.*, 2001] for temperature and salinity from monthly Levitus climatology [*Levitus*, 1982]. Tidal forcing at the open-ocean boundary is decomposed into ten available constituents from TPXO7 [*Egbert et al.*, 1994; *Egbert and Erofeeva*, 2002]. For nontidal forcing at the open-ocean boundary, de-tided daily sea-level observations acquired at NOAA Duck are used. Air–sea fluxes of momentum and heat across the surface of Chesapeake Bay are computed by applying standard bulk formulae [*Fairall et al.*, 2003] to North America Regional Reanalysis from National Center for Environmental Prediction products [*Mesinger et al.*, 2006]. The model integration lasted from 1 September 2011 to 30 June 2012, and was initialized with outputs from a hindcast simulation from 1 January 2010 to 31 August 2011.

[7] The hydrodynamic model is coupled with a sediment transport model developed by *Warner et al.* [2008]. It simulates sediment erosion, suspension, transport, and deposition processes. This coupled hydrodynamic and sediment-transport model has been used to investigate sediment dispersal in the northwestern Adriatic Sea [*Harris et al.*, 2008] and the dispersal of Mississippi and Atchafalaya sediment on the Texas–Louisian shelf [*Xu et al.*, 2011]. The sediment is introduced into the model domain through river and the erosion from the seabed. For the source of fluvial sediment, we only consider the Susquehanna River

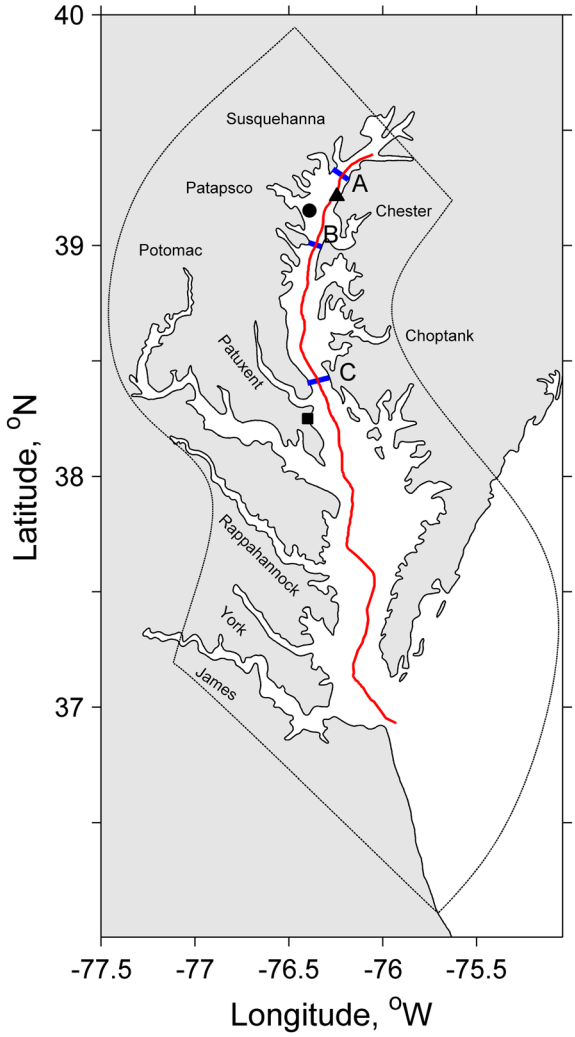

Figure 3. Model domain with the thin dashed lines showing boundaries of the model grid. The red line shows the along-channel axis of the Bay, while the three short blue lines shows three cross-estuary sections selected for sediment flux calculation (marked as A, B, and C). The solid circle marks the location of the Chesapeake Bay Interpretive Buoy, the solid square marks the location of the Patuxent River Naval Air station, and the solid triangle marks NOAA tidal observation station at Tolchester beach.

as it is the only river that discharges sediment directly into the main stem of the Bay while sediment carried by the other tributaries is largely entrapped within them [*Biggs*, 1970; *Schubel and Carter*, 1977]. The fluvial sediment is divided into three classes, i.e., clay, silt, and sand, each represented with a particular grain size. Because this study focuses on fluvial sediment, the seabed is simplified and initialized with uniformly distributed silt that has a single grain size of 0.022 mm [*North et al.*, 2004]. The resuspension of bottom sediment acts as the background for the suspended sediment in the Bay. Relevant parameters of the sediment module are listed in Table 1. For high suspended sediment concentration (SSC), the effect of suspended sediment to water density is included by treating the water as a water–sediment mixture. Although wave-induced shear stress is an important mechanism for sediment erosion in many coastal environments, it is not of the first-order importance here and will not be incorporated into the sediment-transport model since winds over the Bay were weak during the passage of TS Lee and waves are fetch limited in this semi-enclosed estuary.

2.2. Riverine Sediment Input

[8] Measurements of SSC at the Susquehanna River are required to obtain accurate estimates of sediment loading, but no data were collected during TS Lee. We built a regression relation between SSC (in units of mg L^{-1}) and river discharge (R) at Conowingo, Maryland using an extended set of USGS observational data collected between January 1978 and July 2011 [Michael Langland, personal communication] that include runoff R up to 18×10^3 m^3 s^{-1}: $SSC = 21.774 \times \exp(2.2286 \times 10^{-4} \times R) - 15.3107$. The regression coefficient r^2 is 0.79. With this formula, a total of 6.7 million tons of sediment was discharged to Chesapeake Bay between 7 and 17 September. A loading of 5 million tons was obtained using the formula by *Gross et al.* [1978], but we decided to use the former since it is based on recent observations. To focus on the sediment plume generated by TS Lee, the model only considers sediment loading at the Susquehanna River during 6–20 September 2011.

2.3. Model validation

[9] The modeled salinities were validated against the observed surface salinities at the Patapsco River mouth from the Chesapeake Bay Interpretive Buoy System (Figure 4a). The surface salinity showed a rapid drop on 9 September

Table 1. Parameters for the Sediment Transport Model

Sediment Parameters	Fluvial Sediment			Bay Bottom Sediment
	Clay	Silt	Sand	
Grain size (mm)	0.004	0.008	0.069	0.022[a]
Settling velocity (mm/s)[ab]	0.02	0.03	1	0.31
Critical shear stress (N/m^2)[c]	0.013	0.022	0.09	0.049
Erosion constant ($kg/m^2/s$)[a]	4×10^{-5}	4×10^{-5}	4×10^{-5}	5×10^{-5}
Fraction (%)[b]	40	50	10	100
Bottom porosity[d]	0.91	0.91	0.91	0.91

[a]*North et al.* [2004].
[b]*Gross et al.* [1978].
[c]*Gelfenbaum and Smith* [1986].
[d]*Sanford et al.* [1991].

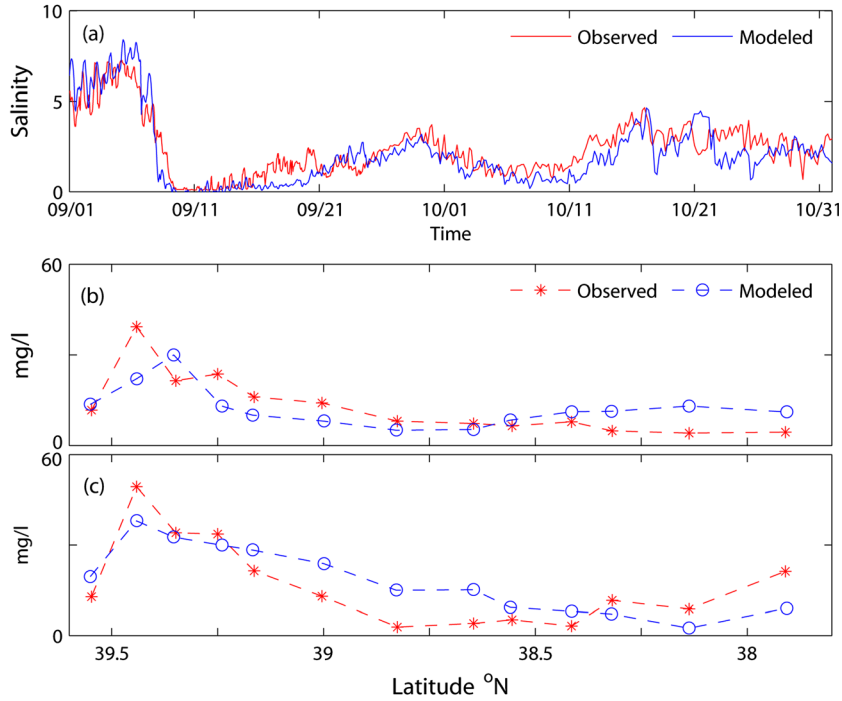

Figure 4. (a) Comparison of the observed (red) and predicted (blue) surface salinity at the location of the Chesapeake Bay Interpretive Buoy. Comparison of the observed (red) and predicted (blue) suspended sediment concentration in the (b) surface and (c) bottom layers in the along-channel section surveyed by the Chesapeake Bay Program.

and remained depressed for 1–2 months. The model accurately captures this observed salinity response. The Root-Mean-Square (RMS) error of the surface salinity is 3.7, and the predictive skill of the model as defined by *Warner et al*. [2005] has a high score of 0.96. The Chesapeake Bay Program measured the total suspended matter concentration at 13 stations along the center axis of the Bay on 19–21 September (see www.chesapeakebay.net). The sediment transport model provides a reasonable prediction for the surface and bottom SSC at these stations (different measurement timing was considered) (Figures 4b and 4c). The RMS error is 0.53 for the surface SSC and is 2.3 for the bottom SSC. The predicted model skills are 0.66 and 0.80 for the surface and bottom SSCs respectively.

3. Results

3.1. Evolution of Sediment Plume

[10] Distributions of daily averaged SSC at the surface and the center axis of the Bay were selected on five particular days to show the temporal evolution of the storm-induced sediment plume (Figures 5 and 6). During summer (July–September), the Susquehanna River flow is relatively low. A gravitational circulation is established in the Bay with a salt wedge lying at 39.2°N. High SSCs are confined to the Bay's head and mouth (Figures 5a and 6a–6c). An estuarine turbidity maximum (ETM) with a maximum SSC of 40–50 mg L^{-1} dominates the upper Bay, as reported in previous observations [*Schubel*, 1968; *Sanford et al*., 1991; *Sanford et al*., 2001]. A secondary maximum of SSC due to tidal resuspension [*Schubel and Carter*, 1977] occurs near the Bay's mouth which is a hotspot of tidal energy dissipation [*Zhong and Li*, 2006].

[11] TS Lee dramatically increased SSC and produced a sediment plume that moved past the ETM region and covered over one half of Chesapeake Bay (Figures 5 and 6). Three stages can be identified in the evolution of the sediment plume, corresponding to three different time scales: $\tau_R = L/U_R$, $\tau_E = L/U_E$, and $\tau_S = H/w_S$ where L is the estuary's length, H is the water depth, U_R, U_E, and w_s represent the velocity scale for the river flow, estuarine circulation, and sediments' settling speed. Using $L = 250$ km, $H = 30$ m, $U_R = 0.75$ m s^{-1}, $U_E = 0.25$ m s^{-1}, and $w_s = 2 \times 10^{-5}$ m s^{-1}, we obtain $\tau_R = 3.8$, $\tau_E = 11.4$, and $\tau_S = 17.4$ days.

[12] During the first stage between 7 and 10 September (Figures 5b and 6d–6f), flood waters forced the salt front seaward by about 30 km as compared to its normal position. On the landward side of the salt front, the normal tidal current pattern was disrupted, and a continuously ebbing current dominated from 9 September to 11 September with a maximum depth-averaged current velocity of roughly 0.8 m s^{-1} during ebb tides in the center channel. SSC exceeded 2500 mg L^{-1} and was nearly uniformly distributed. The high river flow amplified ebb currents and produced strong mixing that helped to suspend sediments in the water column. On the seaward side of the salt front, SSC was low, indicating that the strong salt front acted as a barrier for the seaward sediment transport.

[13] During the second stage between 10 and 18 September, the sediment plume passed beyond the salt front and spread downstream. Turbid water with high SSC reached the mouth of the Patuxent River on 12 September (Figures 5c and 6g–6i). The river discharge dropped to less than 1/2 of the peak value on 11 September and then decreased exponentially (Figure 1b). While the direct river forcing weakened, the

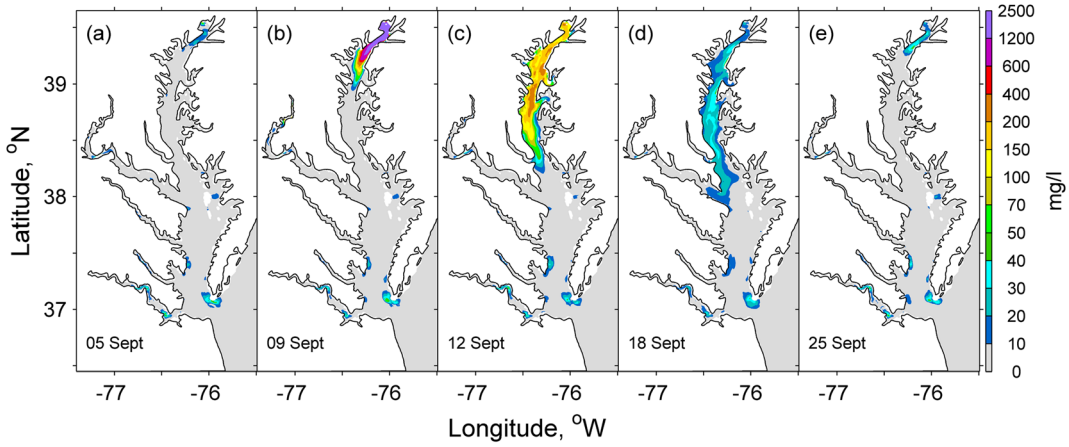

Figure 5. Surface distributions of daily-averaged suspended sediment concentrations on 5 particular days, showing different stages in the temporal evolution of the sediment plume: (a) the pre-storm condition; (b) the seaward push due to river flows; (c) the spreading of the plume by the estuarine exchange flow; (d) precipitation of sediments onto seabed; (e) the post-storm recovered condition.

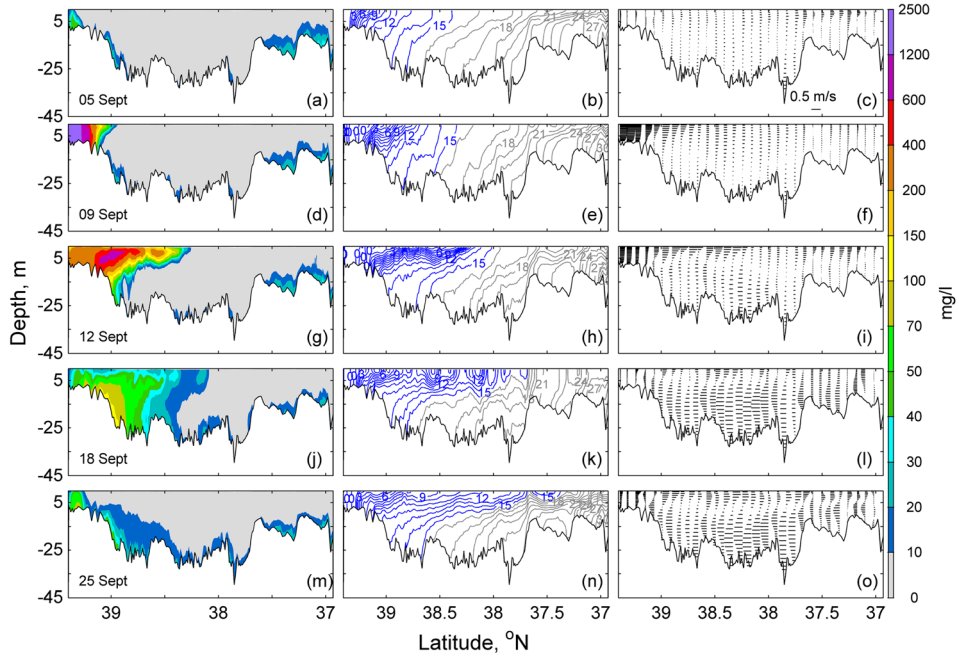

Figure 6. Daily averaged suspended sediment concentrations (left column, color bar on the far right), salinity distributions (at 1 psu intervals, middle column), and along-channel current (right column) in the along-channel section on 5 particular days, showing different stages in the development of the sediment plume. The first panel shows the pre-storm condition, and the last panel shows the recovered condition after the storm. Panels 2–4 show three stages in the evolution of the sediment plume during TS Lee.

large horizontal salinity gradient forced the estuary to reestablish the stratification. The bottom salty water began to move upstream and restored to its previous position. The two-layer circulation strengthened substantially, with strong surface currents reaching over 0.3 m s^{-1}. As a result, the fluvial sediments were mostly advected downstream along with the freshwater in the upper water column. The center of the sediment plume left the head of the Bay and shifted to the eastern shore of the Bay around 39°N. The SSC of the plume dropped to below 600 mg L^{-1}, mostly due to settling and partly due to dilution of seawater.

[14] In the third stage between 18 and 25 September, the settling became the dominant process. Large amounts of fluvial sediment were settling down onto the seabed, while the rest in the surface layer were advected seaward (Figures 5d and 6j–6l). Maximum SSC dropped to less than 100 mg L^{-1}, which is close to the largest SSC produced by tidal resuspension in the turbidity maximum under normal conditions [*Schubel*, 1968]. A strong northerly wind blew down the Bay on 15–18 September (Figure 1a) and amplified the two-layer circulation, thus dispersing the sediment plume further south [e.g., *Chen and Sanford*, 2009]. The

farthermost front of the sediment plume approached the mouth of the Rappahannock River, and the center of the turbid water was confined near the western shore of the middle Bay due to the earth's rotation. Moreover, the sediment plume penetrated far into the Potomac River, acting as a sediment source for the river. The along Bay axis profile of SSC shows an opposite distribution to that of tidal resuspension with higher SSC near the surface as a result of settling. It is somewhat surprising that the time scale for sediment deposition is not longer than the simple scaling $\tau_S = H/w_S$ that ignores the effects of turbulent diffusion. One plausible explanation is that turbulent mixing was strongly suppressed by the restratification and did not delay the vertical settlement of sediments.

[15] After 25 September, the sediment plume retreated to the upper Bay (Figures 5e and 6m–6o). Most of the fluvial sediments had settled on the seabed, while higher SSC was found near the bottom. SSC distribution in the Bay restored to the pre-storm conditions. The ETM in the upper bay and the secondary maximum SSC near the Bay's mouth appeared as the dominant features in the surface distribution of SSC.

[16] The sediment plume generated by TS Lee never reached the shelf but remained trapped inside the estuary. To characterize the relative importance of horizontal advection and vertical sinking in the spreading of suspended sediment, *Geyer* [1993] defined a dimensionless trapping length, $l = u_1 h_1 / w_s L$ where u_1 and h_1 are the velocity and thickness of the upper estuarine layer, w_s is settling velocity, and L is the length of the salinity intrusion (or estuarine length). This parameter is the ratio of the advective length scale for sinking of sediment out of the upper layer to the length of the estuarine convergence zone. Taking $h_1 = 10$ m, $u_1 = 0.25$ m s^{-1}, and $w_s = 2 \times 10^{-5}$ m s^{-1}, we obtain $l = 0.5$. Hence, Chesapeake Bay is an estuary that traps sediment and our model result is in agreement with Geyer's prediction.

3.2. Longitudinal Flux of Suspended Sediment

[17] Figures 5 and 6 show that the river flow and estuarine exchange flow play important roles in transporting the sediment plume down the estuary. For a scalar such as salt or sediment, three advective processes drive the longitudinal transport in the estuary: the freshwater outflow that tends to drive sediment out of the estuary, the estuarine exchange flow that disperses sediment through shear flow dispersion, and tidal dispersion owing to the covariance between SSC and tidal currents. We can examine their relative contributions to the longitudinal suspended sediment transport by adapting a salt flux decomposition method of *Lerczak et al.* [2006]. The total suspended sediment flux (F_S) at a cross-estuary section can be decomposed into three components,

$$F_s = \left\langle \iint (u_0 C_0 + u_E C_E + u_T C_T) dA \right\rangle = F_0 + F_E + F_T, \quad (1)$$

where the angled brackets indicate a low-pass, subtidal temporal filter (here, we use a filter with a half-period at 34 hours), u is the along-estuary velocity, C is the SSC for a particular grain size, A is a unit area of the cross section, F_0 is the sediment flux transported by freshwater outflows or wind-driven barotropic flows [e.g., *Jia and Li*, 2012], F_E is the sediment flux resulting from subtidal shear dispersion, and F_T is the tidal oscillatory sediment flux. Both u and C are separated into three components: tidally and cross-sectionally averaged, tidally averaged and cross-sectionally varying, and tidally and cross-sectionally varying, representing with subscript 0, E, and T, respectively. The definitions of the three components are:

$$\phi_0 = \frac{1}{A_0} \iint \langle \phi(y,z) \rangle dA, \quad (2)$$

$$\phi_E(y,z) = \frac{\langle \phi A \rangle}{\langle A \rangle} - \phi_0, \quad (3)$$

$$\phi_T(y,z,t) = \phi - \phi_0 - \phi_E, \quad (4)$$

where ϕ represents either u or C, y and z are cross-estuary and vertical coordinates respectively, and A_0 is the low-passed total cross-sectional area.

[18] We select three cross sections to investigate the longitudinal sediment flux: one located near the head of estuary (Section A), one near the Bay Bridge (Section B), and one near the end of the sediment plume (Section C), respectively (see Figure 3 for their locations). We use the clay component as an example for the flux calculation since the result for the silt component is similar and most of fast-sinking sands were trapped near the estuary's head. First, it is interesting to note that the three flux components were all negative during TS Lee, demonstrating that all three advective processes contributed to the seaward sediment transport. At Section A in the ETM region, the freshwater outflow was the dominant transporter of suspended sediment and accounted for nearly 71% of the total clay flux. The estuarine exchange contributed about 29%, while the tidal dispersion was negligible (Figure 7a). As shown in Figure 6, the salt front was pushed seaward by the strong river flow so that the freshwater outflow overwhelmed the estuarine exchange flow in transporting the sediment. Tidal pumping of suspended sediment was also weak there. At Section B near the Bay Bridge, the freshwater outflow was still a major transporter

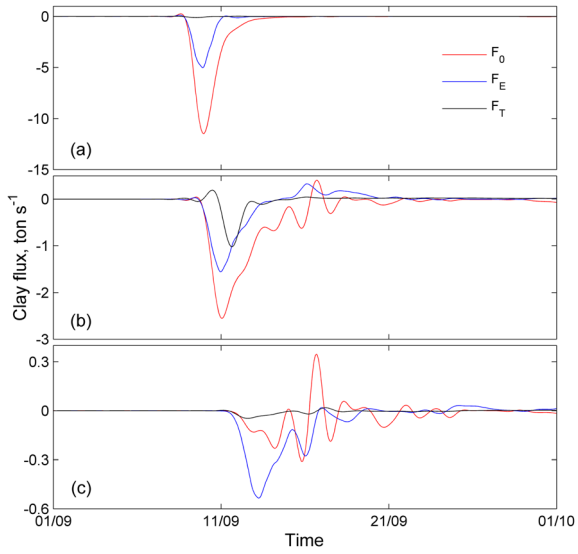

Figure 7. Decomposition of longitudinal suspended sediment flux at three cross sections whose locations are marked in Figure 3: (a) section A; (b) section B; and (c) section C. F_0 is the sediment flux due to freshwater outflow and wind-driven barotropic transport, F_E is the sediment flux due to estuarine exchange flow, and F_T is tidal dispersion of sediment.

of sediment but the estuarine exchange flow and tidal dispersion made significant contributions to the seaward sediment transport (Figure 7b). The strong tidal dispersion of suspended sediment might result from the large tidal variations of SSC. At Section C which lies north to the mouth of the Patuxent River, the clay flux carried by the estuarine exchange flow exceeded that due to the freshwater outflow, and tidal dispersion became negligible again due to weak tides in the mid-Bay (Figure 7c). Around 15 September, a strong northerly wind event (see Figure 1a) caused seaward barotropic flux (F_0) during wind setup and landward flux during wind setdown, as shown in previous studies of wind effects on the salt flux [e.g., *Li and Li*, 2011]. The above analysis shows that the river flow dominates the downstream sediment transport in the upper Bay whereas the estuarine exchange flow dominates the longitudinal sediment transport in the mid-Bay. In this mid-Bay region, the sediments will be transported seaward when they remain suspended in the surface layer but will be transported landward when they sink to the bottom layer.

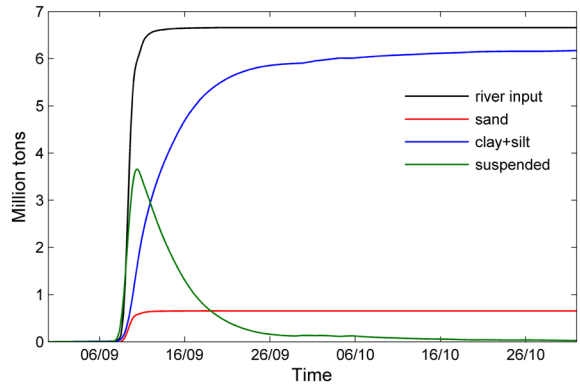

Figure 8. Time series of the time-integrated sediment budget for Chesapeake Bay: the accumulative sediment input from the Susquehanna River (black); the total mass of suspended sediments in the Bay (green); the accumulative deposits of sands (red), and clays and silts (blue) on the seabed.

3.3. Deposition of Flood Sediments

[19] To know the fate of the suspended sediment, we calculate the total sediment budget for Chesapeake Bay

$$\frac{dM_s}{dt} = F_R - F_{sand} - F_{clay+silt} - F_{out}, \tag{5}$$

where M_s is the total suspended sediment in the Bay, F_R is the sediment flux from the Susquehanna River, F_{sand} is the net deposition flux (i.e., sum of deposition and erosion) for sands and $F_{clay+silt}$ is the net deposition flux for clay and silts, and F_{out} is the sediment outflux to the adjacent shelf. Figure 8 shows the time series of the time-integrated sediment budget between 1 September and 31 October 2011. During 7 to 17 September, the total input of fluvial sediments $\int_0^t F_R dt$ from the river reached 6.7 million tons. At the peak river discharge, over 55% of the sediments were suspended in the water column while the rest settled onto the seabed. M_s reached a maximum of 3.9 million tons on 12 September and took almost a month to recover to the pre-storm value. The deposition of fine-grained fluvial sediments (clay and silts) $\int_0^t F_{clay+silt} dt$ showed a mirror image to M_s after 12 September. Given a water depth of 30 m, it takes nearly 11 days for the silts and 17 days for the clays to settle onto the bed. This is consistent with an accumulation time of 2–3 weeks for the fine-grained sediment (Figure 6). Due to the relatively large settling velocity (1 mm s^{-1}), the sands sank down 30 m depth in 8 h so that $\int_0^t F_{sands} dt$ reached a steady state quickly. Based upon the budget calculations, we estimate that 6.56 million tons of fluvial sediment had deposited inside Chesapeake Bay by 25 September, 0.14 million tons remained suspended in the water column, and none exported to the shelf.

[20] The deposition of flood sediments showed distinct spatial patterns (Figure 9a). Most sediments were deposited in the upper Bay, with a maximum thickness of new sediment

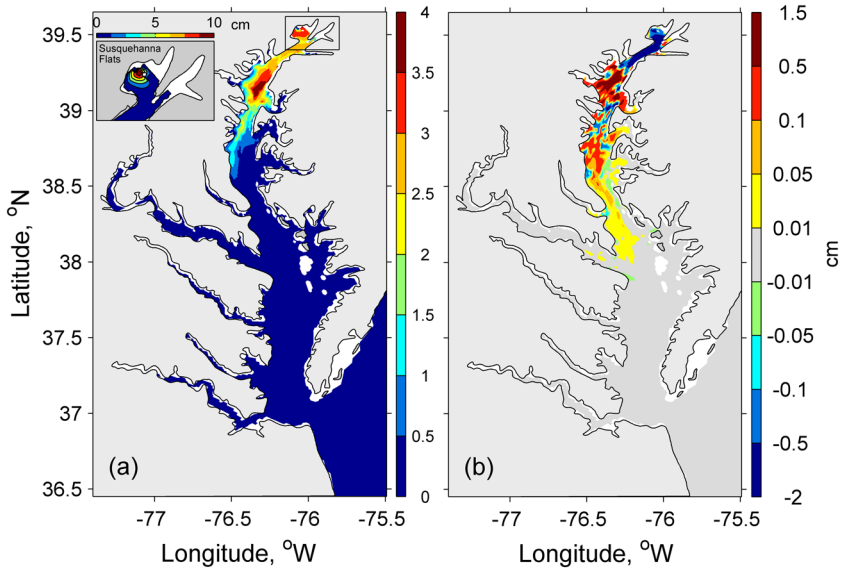

Figure 9. (a) Thickness of fine-grained (clay and silt) flood sediment on 25 September 2011. The insert shows the thickness of the sand deposition on the Susquehanna Flats. (b) The difference in the thickness of fine-grained flood sediment between 30 June 2012 and 25 September 2011.

of nearly 15 cm near the mouth of the Susquehanna River. This is similar to the deposition pattern produced by Tropical Storm Agnes [*Schubel and Zabawa*, 1977]. The sands were mainly dumped near at the Susquehanna Flats with a maximum thickness of 10 cm, while the fine-grained fluvial sediments were dusted in the northern part of the Bay and exhibited clear cross-estuary variability. In the upper Bay (above Bay Bridge), most fine-grained sediments accumulated near the eastern shore with a maximum thickness of 4 cm above the mouth of the Chester River. In the mid-Bay, the deposition of fine-grained sediment was constricted to the western shore with a thickness of 1.5 cm.

[21] The sediments that had deposited onto the seabed during TS Lee may be mobilized by tidal flows and transported to other regions after the storm. To find out the ultimate fate of the storm sediments, we extended the model integrations to June 2012 and compared the distribution of the sediment deposition on the seabed between 25 September 2011 and 30 June 2012 (Figure 10). Most sands were deposited in the Susquehanna Flats during the storm and remained there 10 months later. The net change in the thickness of the sand layer was less than 0.1 cm. However, significant changes in the distributions of deposited clay and silt layers occurred between September 2011 and June 2012 (Figure 10). The 1 cm thick clay layer that was deposited north of 39.3°N disappeared by June 2012, while the clay layer became thicker south of 39.3°N. Similarly, the silt layer became thinner in some northern parts of the upper Bay, although some silts remained deposited in the area of the Susquehanna Flats. A notable feature is that both clay and silt depositions reached their maximum thicknesses in the ETM region. This suggests that the ETM provided an effective trap for many of the flood sediments during the post-storm period. A detailed discussion on the ETM trapping mechanism will be presented in section 4.1. To better visualize the long-term changes in the sediment deposition, we plot the difference in the thickness of the fine-

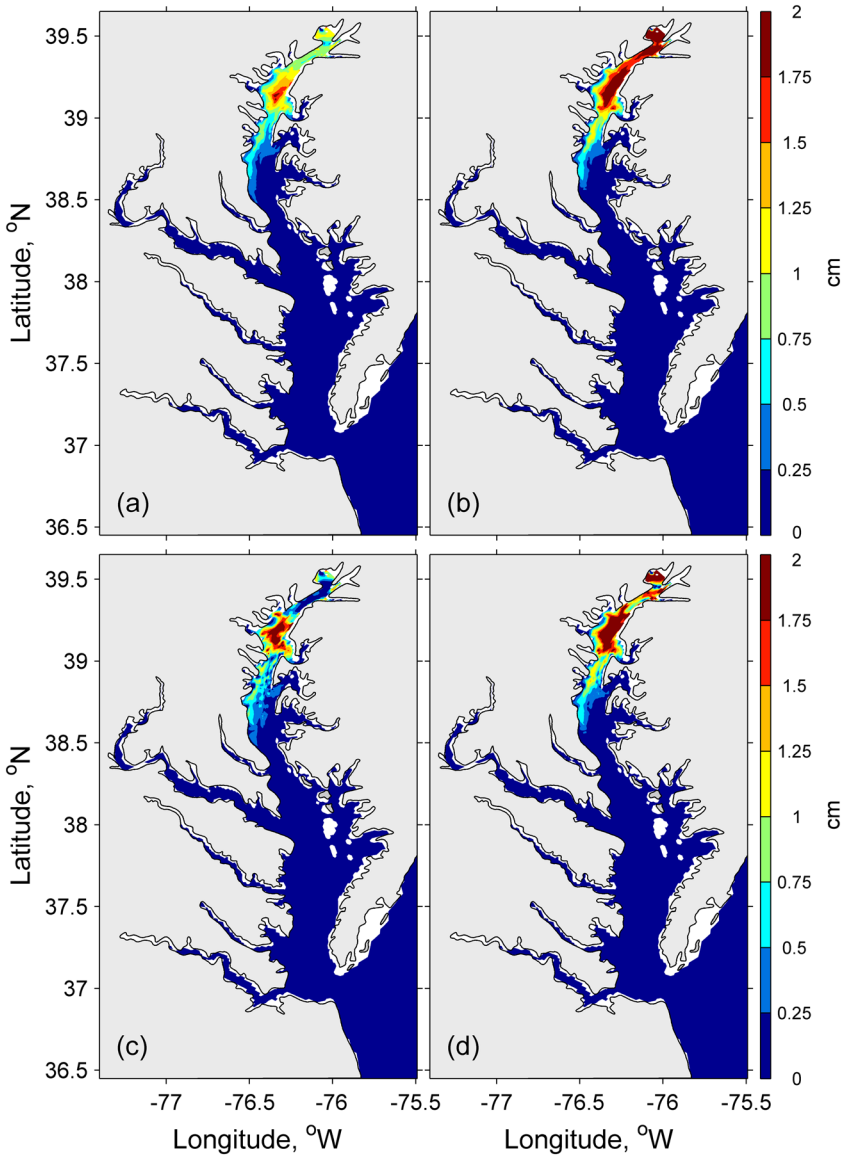

Figure 10. Thickness of the (a/c) deposited clay and (b/d) silt layer on the sea bed: (top) 25 September 2011 and (bottom) 30 June 2012.

grained (the sum of clay and silt components) bottom sediments between 30 June 2012 and 25 September 2011 (Figure 9b). North of 39.3°N, the thickness of bottom sediment decreased by about 2 cm, indicating that most of the flood sediments could be eroded within a year, and continuous riverine input is needed to maintain the sediment pool there. South of 39.3°N, the thickness of bottom sediment generally increased, with a maximum gain of 1.5 cm.

[22] Some flood sediments appear to have migrated further seaward, as shown in Figure 9b. The thickness of the clay and silt layer increased by 0.1–0.5 mm between 38.0 and 38.6°N and by 1–5 mm between 38.6 and 39.1°N. Resuspension of fine-grained sediments by tidal flows together with advection by two-layer estuarine flows are likely responsible for this post-storm redistribution of sediments. The sediments that deposited south of the ETM region during TS Lee can be suspended by strong tidal currents since the maximum bottom tidal stress exceeds the critical shear stress for the sediment suspension. If the sediments are suspended in the lower layer, the landward estuarine flow will transport them upstream to the ETM region. If they are diffused into the upper layer, however, the seaward estuarine flow will transport them downstream so that they will be deposited further seaward. It is possible that a small percentage of the flood sediments may eventually winnow out the estuary and spill out onto the adjacent shelf, but most of the sediments should remain trapped inside the estuary.

4. Discussions

4.1. Effectiveness of ETM in Trapping Sediments During the Storm

[23] The model results showed that most sands and some silts were trapped and deposited near the ETM zone, whereas clays and some silts were transported further downstream. *Sanford et al*. [2001] reported similar observations: a large flood event in January delivered most of the sediment load beyond the ETM, while suspended sediments delivered during a flood event in October were trapped efficiently in the ETM. They attributed the difference in sediment trapping to increases in particle settling speed from January to October. To better understand why the ETM did not trap fine-grained sediments during TS Lee, we have conducted a diagnostic analysis of the SSC equation.

[24] The creation of ETM has been attributed to convergence of gravitational circulation [*Postma*, 1967; *Festa and Hansen*, 1978] and estuarine stratification that enhances the trapping of suspended sediment on the seaward side of the salt front [*Geyer*, 1993]. The importance of tidal forcing was recognized by *Schubel* [1968] who suggested that the elevated SSC in ETM is maintained by tidal resuspension. *Jay and Musiak* [1994] introduced the concept of internal tidal asymmetry and proposed that tidal asymmetry in turbulent mixing is the major mechanism producing ETM. Using a conceptual diagram, *Sanford et al*. [2001] illustrated that flood–ebb asymmetries in tidal resuspension and transport are mainly responsible for the maintenance of the ETM in the upper Chesapeake Bay. Insights into the ETM's sediment trapping mechanisms can be gained by comparing key terms in the transport equation for the suspended sediment:

$$\frac{\partial C}{\partial t} = -\frac{\partial uC}{\partial x} - \frac{\partial vC}{\partial y} - \frac{\partial wC}{\partial z} + \frac{\partial w_s C}{\partial z} + \frac{\partial}{\partial z}\left(K_s \frac{\partial C}{\partial z}\right), \quad (6)$$

where u, v, and w are velocities in the along-estuary (x), cross-estuary (y), and vertical directions (z), w_s is the settling velocity of a particular grain size, and K_s is the vertical eddy diffusivity. Since the axial dynamics in the channel dominates particle trapping processes in the Chesapeake Bay ETM [*Sanford et al*., 2001], the lateral transport of suspended sediment will be not considered (e.g., the second and third terms on the right hand of equation (6)). The settling velocity for clays and silts is small and thus neglected. Hence, we focus our analysis on the role of longitudinal advection and vertical diffusion in the ETM formation.

[25] We first analyze nonflood periods to illuminate the ETM trapping mechanism. We selected a tidal cycle during the neap tide (10 October 2011) (see Figure 1). Figures 11a–c show intra-tidal variations of the longitudinal bottom shear stress, depth-averaged absolute value of vertical diffusion term, and the depth-averaged longitudinal advection term along the center axis in the upper Bay. The bottom stress exhibited a pronounced asymmetry between the flood and ebb tides. In the southern part of the upper Bay (south of 39.22°N which is the approximate location of the estuarine salt front), the bottom shear stress is stronger on flood than on ebb, showing a typical tidal asymmetry in an estuary. In the northern part of the upper Bay (north of 39.22°N), however, the bottom stress is weaker on flood than on ebb, showing a reversed tidal asymmetry. This reversed tidal asymmetry occurs since the water column becomes stratified during the flood tide due to the upstream advection of stratified water but is well mixed during the ebb tide due to the downstream advection of freshwater [*Fugate et al*., 2007]. As shown in Figure 11b, the vertical diffusion of sediment in this northern part of the upper Bay is significantly larger on ebb than on flood, indicating that more sediments are introduced into the water column during the ebb tide. The longitudinal advection is seaward on ebb and landward on flood (Figure 11c). Therefore, the combined effect of tidal asymmetries in vertical diffusion and longitudinal advection is to erode bottom sediment in the northern upper Bay and move it downstream. This result is consistent with the conceptual diagram of *Sanford et al*. [2001]. In the upper Bay region south of 39.22°N, however, tidal asymmetries in the vertical diffusion and longitudinal advection of suspended sediment are opposite to those in the region north of it so that the sediment is transported upstream. Therefore, the temporal and spatial variations of sediment resuspension and advection lead to a bottom sediment pool near the upper limit of salt intrusion and high SSC in the ETM.

[26] The analysis of a tidal cycle during the spring tide (on 30 September 2011) is shown in Figures 11d–f. The spring tide pushed the salt front further landward, but the elevated river flow pushed it seaward. The net result is that the salt front shifted slightly upstream to 39.29°N. Although the magnitude of bottom shear stress and vertical diffusion were larger during the spring tide than during the neap tide, the effects of internal tidal asymmetry on the sediment transport are similar to those seen during the neap tide. North of the salt front, the "reversed" flood–ebb asymmetry in bottom stress, and turbulence diffusion resulted in a net seaward sediment transport over a tidal cycle. South of the salt front, however, the "normal" flood–ebb asymmetry in vertical

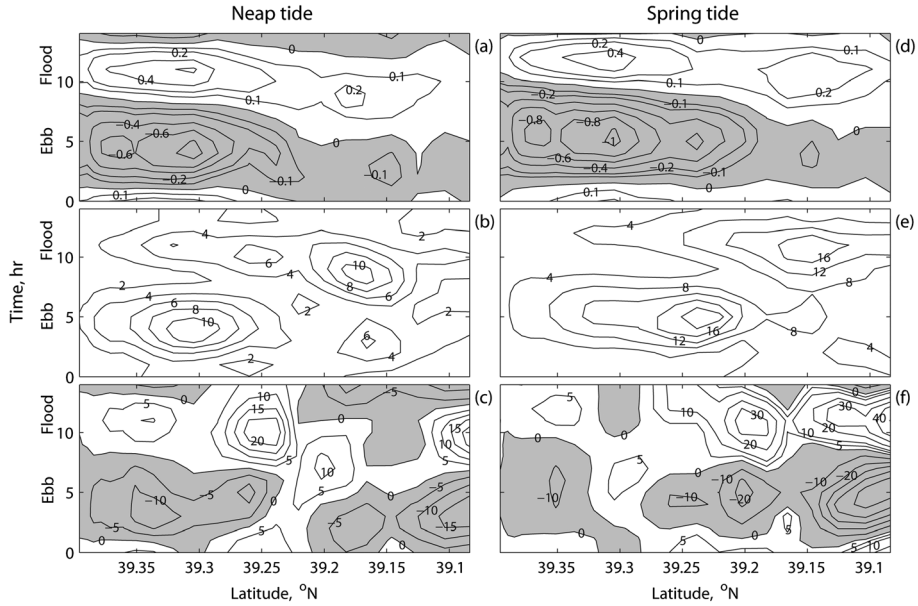

Figure 11. Bottom shear stress (the first row) and diagnostic terms in the suspended sediment transport equation over one tidal cycle during the neap (10 October 2011) and spring (30 September 2011) tides, respectively. The second row shows the depth-averaged amplitude (absolute value) of vertical diffusion term, and the third row shows the depth-averaged longitudinal advection term. The diagnostics terms are in units of 10^{-7} kg m^{-3} s^{-1}.

mixing and longitidunal advection led to a net landward sediment transport. This flood–ebb asymmetry in tidal suspension and advection as well as the convergence of the estuarine circulation are responsible for the post-storm accumulation of the storm-delivered sediments at the ETM region, as shown in Figure 10.

[27] Now we show a similar diagnostic analysis of the SSC equation during TS Lee (Figure 12). We have selected two tidal cycles on 12 September 2011 for the analysis and extended the southern boundary to 38.5ºN since the sediment plume had reached this latitude (see Figure 5c). The large river flow not only pushed the salt front downstream to about 38.7ºN (Figure 6h) but also fundamentally changed the flood–ebb tidal flow patterns north of this latitude. The ebb tides were much stronger than the flood tides. Consequently, the bottom shear stress and water-column turbulence diffusion were stronger on ebb than on flood over an extended region between the estuary's head and 38.7ºN. The tidally averaged longitudinal advection of sediment is directed downstream. South of the salt front, the bottom stress was stronger on flood than on ebb, exhibiting the flood–ebb tidal asymmetry expected in an estuary. However, the magnitude of depth-averaged vertical diffusion of suspended sediment did not show significant flood–ebb asymmetry, despite that the eddy diffusivity in the tidal bottom boundary layer is larger on flood. As shown in Figure 6g, the slow-sinking clays and silts remained suspended in the surface layer where tidal asymmetry in turbulent mixing is not significant. More interestingly, the longitudinal sediment flux was negative during most of the tidal phases, indicating that suspended sediment was predominantly transported seaward. In summary, the fine sediments delivered by TS Lee moved past the ETM region

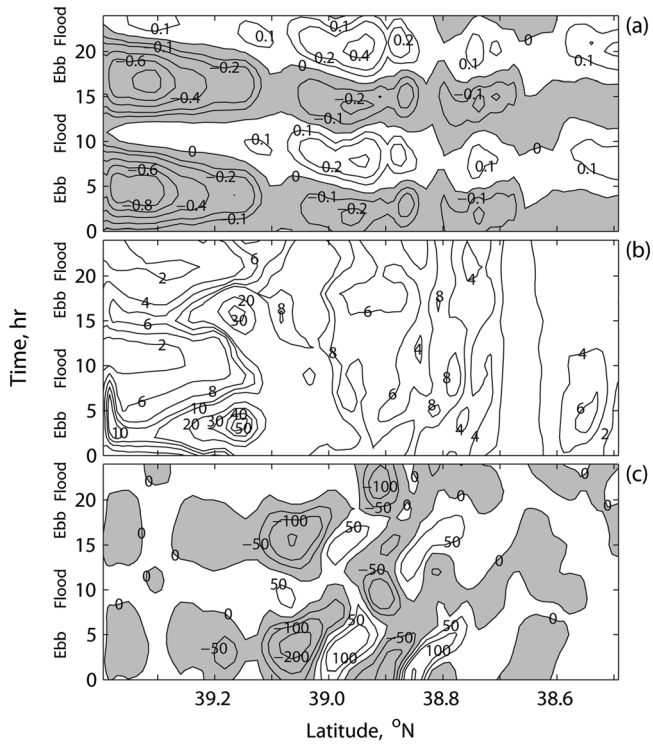

Figure 12. (a) Bottom shear stress during 12 September 2011. Diagnostic terms in the suspended sediment transport equation: (b) the depth-averaged amplitude (absolute value) of vertical diffusion term and (c) the depth-averaged longitudinal advection term. The diagnostics terms are in units of 10^{-6} kg m^{-3} s^{-1}.

because they were suspended in the surface layer and transported downstream by seaward estuarine currents. Unlike a typical ETM, sediment resuspension by tidal flows was not an important factor.

4.2. Sensitivity to Sediment Parameters

[28] The numerical simulation of the sediment plume is sensitive to sediment parameters. To find appropriate settling velocities for the flood-delivered sediment, we carried out a series of sensitivity-analysis experiments. At smaller settling velocities, the sediment plume extended farther seaward, and less flood sediments were trapped in the ETM. We selected the settling velocities that gave the best prediction for the along-estuary distribution of SSC (see Figures 4b and 4c). The numerical model assumed constant settling velocities for each sediment class and neglected effects of flocculation that could be important during large floods [*Hill et al*., 2000]. The observed settling velocity of sediment flocs ranges from 0.3 mm s^{-1} to 3 mm s^{-1} in the ETM region of Chesapeake Bay [*Sanford et al*., 2001]. We ran the model with the settling velocity in this range and found that almost all of the flood sediments were trapped near the head of the Bay, similar to the distribution of the sand component. A wide range of the settling velocity, therefore, is expected for the flood-borne sediments. One approach to consider the effects of flocculation would be to use an empirical formula of the flocs's settling velocity that varies with SSC and turbulence dissipation rate or shear-stress magnitude [*Burban et al*., 1990; *Partheniades*, 1992]. However, we cannot easily incorporate such a formula into ROMS because the calculation of sediment settling is based on a semi-Lagrangian method. Settling velocities also influence the intra-tidal variation of ETM. Due to asymmetries in tidal mixing, the settling velocity varies during a tidal cycle because stronger turbulent mixing tends to break flocs. The tidal asymmetry in sediment settling velocity, which may help develop ETM, was neglected in the numerical model and in the above analysis of ETM.

[29] Another important sediment parameter is the critical shear stress for each grain size. We chose their values by following a nondimensional Sheilds curve that assumes noncohesive well-sorted particles [*Gelfenbaum and Smith*, 1986]. We conducted a sensitivity experiment in which the critical shear stress of each grain size is doubled. We found a deposition pattern of the flood sediment (on 25 September 2011) that is similar to Figure 9a because deposition overwhelmed erosion during the flood period. The redistribution of flood sediment between September 2011 and June 2012 is also similar, although less sediments were mobilized by tidal currents due to the larger threshold of the shear stress. The critical shear stress was assumed spatially uniform throughout the Bay for each grain size, and the consolidation and armoring effect were neglected. Sediment erodibility experiments showed that the critical shear stress varies significantly in the upper Chesapeake Bay in response to consolidation and swelling processes [*Sanford and Maa*, 2001]. Estimates of the critical stresses for erosion of mid-Bay silts range from 0.12 N m^{-2} at the sediment surface to 0.3 N m^{-2} at about 1 mm sediment depth [*Sanford*, 2006]. In future work, one may incorporate the multilayer sediment bed model of *Sanford* [2008] that provides the first-order treatment for consolidation, armoring and bioturbation.

[30] Due to the high SSC during the flood, suspended sediment might affect the density of water–sediment mixture. We have compared two model runs with and without considering the sediment contribution to water density and found minor differences in water-column stratification and current velocities. The contribution of suspended sediment is included in the equation of state for seawater density as:

$$\rho = \rho_{water} + C\frac{\rho_{sed} - \rho_{water}}{\rho_{sed}}, \tag{7}$$

where ρ is the density of water–sediment mixture, ρ_{water} is the water density, $\rho_{sed} = 2650$ kg m^{-3} is the sediment density, and C is SSC [*Warner et al*., 2008]. Given the maximum SSC (2.5 g L^{-1}) of the flooding water, the suspended sediment produced a density anomaly of 1.56 kg m^{-3} that is equivalent to a change in salinity of 2 psu. In the seaward side of the salt front, the SSC generally was less than 1 g L^{-1}, and its contribution to water density is smaller than that due to 0.8 psu salinity, while the vertical salinity difference was generally larger than 10 psu (Figure 6).

4.3. Impacts on Ecosystem

[31] We have shown that TS Lee discharged over 6.7 million tons of suspended sediments into Chesapeake Bay. This is equal to the input of 6 average years [*Gross et al*., 1978]. Such extreme flood events not only have a great impact on the sedimentary history of Chesapeake Bay but also may affect water quality and ecosystem productivity in the estuary. High SSCs degrade water clarity, threatening phytoplankton photosynthesis, and submerged aquatic vegetation. Organic materials and nutrients associated with the sediments provide extra nutrients to the eutrophic system and may lead to worse hypoxia.

[32] The growth rate of phytoplankton depends on the photosynthetically available radiation that is controlled by the light attenuation coefficient, K_d. *Xu et al*. [2005] obtained an empirical formula of K_d for Chesapeake Bay as a function of *chlorophyll a* concentration, salinity, and SSC. We use the empirical formula of *Xu et al*. [2005] and the model-predicted SSC to estimate the light attenuation coefficient K_d during TS Lee. The average K_d in the northernmost region (region 6 as defined in *Harding et al*. [2002]) reached a peak value of 50 m^{-1} on 9 September and decreased to 5 m^{-1} on 14 September. The average K_d in the second northernmost region (region 5) reached a maximum of 10 m^{-1} on 11 September and decreased slowly with time. They are much larger than typical K_d values of 1–2 m^{-1}. Thus, the sediment loading due to TS Lee severely impaired light in Chesapeake Bay for about 2 weeks.

[33] According to the deposition pattern of the fluvial sediment (e.g., Figure 9a), submerge aquatic vegetation, one of the few bright spots in the restoration of Chesapeake Bay, might be damaged severely at the Susquehanna Flats since all of sand component and large portion of silt component were deposited in this area, but would suffer less impairment in other parts of the northern Bay as the fine-grained sediments spread over a wide area as a relatively thin layer. The damage to the submerged aquatic vegetation also depends on the timing of storm relative to its growing season. Numerical experiments showed that a storm in September not only reduces submerged aquatic vegetation

shoot biomass in September, but also reduces submerged aquatic vegetation biomass in the next year due to the lower shoot survival during the winter [*Wang and Linker*, 2005].

[34] The Susquehanna River is the largest single source of nutrients to Chesapeake Bay, carrying over 70% of the total nitrogen and 55% of the total phosphorus [*Smullen et al*., 1982]. According to the USGS long-term data set (available at http://va.water.usgs.gov/chesbay/RIMP/loads.html), the average nitrogen and phosphorus contents of the Susquehanna River sediment during the recent decade (2001–2010) are estimated to be 1.73% and 0.21%, respectively. Hence, about 115,910 tons of particulate nitrogen and 14,070 tons of particulate phosphorus were discharged into the Bay during TS Lee. The average annual inputs of total nitrogen and phosphorus associated with sediment from all tributaries are estimated to be 151,680 and 11,250 tons, respectively [*Boynton et al*., 1995]. Hence, TS Lee delivered about 9 month supply of particulate organic nitrogen and over 1 year supply of particulate organic phosphorus to the Bay. Using the average concentrations of dissolved inorganic nitrogen of 1.5 mg L^{-1} and dissolved inorganic phosphorous of 0.025 mg L^{-1} recorded at USGS monitoring stations during the storm, we estimate that TS Lee delivered 10,763 tons of dissolved nitrogen and 183 tons of dissolved phosphorous to the Bay. These compare with the average annual loadings of dissolved nitrogen of 44,360 tons and dissolved phosphorus of 410 tons. Hence, TS Lee delivered 2.5 average months of dissolved inorganic nitrogen and 4.5 average months of dissolved inorganic phosphorus to Chesapeake Bay. Post-storm survey revealed that hypoxia returned after TS Lee's passage [Mike Roman, personal communication]. It is quite possible that the excess nutrients delivered by the storm may lead to high phytoplankton production and worse hypoxia. Further investigations using coupled hydrodynamic-biogeochemical models would be useful to understand the impacts of TS Lee on the plankton productivity and water quality in Chesapeake Bay.

5. Conclusions

[35] During TS Lee, the Susquehanna River discharged about 6.7 million tons of suspended sediment into Chesapeake Bay, a mount equivalent to the input of 6 average years [*Gross et al*., 1978]. Such extreme flood events not only have a great impact on the sedimentary history of Chesapeake Bay but also may affect water quality and ecosystem productivity in the estuary.

[36] Using a numerical model, we simulated TS Lee-induced sediment plume that underwent through three stages, each dominated by a particular process. The freshwater outflow dominated the first stage, the estuarine exchange flow dominated the second stage, and settling dominated the third stage. The analysis of longitudinal suspended sediment flux at three cross sections showed that different regions of the sediment plume were controlled by different mechanisms of sediment transport. The freshwater outflow was responsible for most of the seaward sediment transport in the upper Bay whereas the estuarine exchange flow was responsible for the longitudinal sediment flux in the mid-Bay.

[37] Most of the flood sediments were deposited in the upper bay during TS Lee: all sands and some silts were dumped in the Susquehanna Flats, while clays and some silts were dusted over a wide area in the upper Bay. Long-term model integration showed that the ETM acted to trap a large amount of the flood sediments. We conducted a diagnostic analysis of the suspended sediment transport equation and found that tidal asymmetries in resuspension and transportation are the primary process transporting sediment toward the salt front. Ebb-enhanced bottom stress and turbulent diffusion on the landward side of the salt front led to a seaward migration of the storm sediments. In contrast, flood-enhanced bottom stress and turbulent diffusion on the seaward side of the salt front resulted in a landward transport of sediments. Although most of the flood sediments were trapped in the ETM, a small amount of fine-grain sediments (clays and some silts) were transported seaward onto the mid-Bay.

[38] With global warming, both the frequency and intensity of tropical storms have increased notably during the past decades [*Emanuel*, 2005]. The Chesapeake Bay region is expected to encounter more inundation, high winds, and floods in future. The impacts of tropical storms on an estuary may be categorized into two types. For dry storms such as Hurricanes Isabel (2003) and Irene (2011), the main impacts are storm surges and strong wind mixing which may ventilate bottom water and bring temporary relief to hypoxia. For wet storms such as Tropical Storms Agnes (1972) and Lee (2011), however, the main impacts are extreme river discharge and massive loading of terrestrial materials such as sediments and nutrients. Although the second type of the storms may bring less direct damage to human populations, it probably poses more serious threats to water quality and ecosystems in estuaries and coastal oceans.

[39] **Acknowledgments.** We are grateful to Michael Langland for providing the data on the sediment loading at the Susquehanna River, and Walter Boynton and Chesapeake Bay Program for providing the survey data on suspended sediments. We thank Larry Sanford, Cindy Palinkas, and Jeff Brainard for helpful discussions and two reviewers for their insightful comments. This work is supported by NSF grant OCE-0825453. This is UMCES contribution number 4721.

References

Biggs, R. B. (1970), Sources and distribution of suspended sediment in northern Chesapeake 311 Bay, *Marine Geol.*, *9*, 187–201.

Boynton, W. R., J. H. Garber, R. Summers, and W. M. Kemp (1995), Inputs, transformations, and transport of nitrogen and phosphorus in Chesapeake Bay and selected tributaries, *Estuaries*, *18*, 285–314.

Burban, P. Y., Y. Xu, J. McNeil, and W. Lick (1990), Settling speeds of flocs in fresh and sea Waters, *J. Geophys. Res.*, *95*(C10), 18,213–18,220.

Chen, S.-N, and L. P. Sanford (2009), Axial wind effects on stratification and longitudinal salt transport in an idealized, partially mixed estuary, *J. Phys. Oceanogr.*, *39*, 1905–1920.

Egbert, G. D., Bennett, A., and M. Foreman (1994), TOPEX/Poseidon tides estimated using a global inverse model, *J. Geophys. Res.*, *99*(C12), 24,821–24, 852.

Egbert, G. D., and S. Y. Erofeeva (2002), Efficient inverse modeling of barotropic ocean tides, *J. Atmos. Oceanic Technol.*, *19*(2), 183–204.

Emanuel, K. A. (2005), Increasing destructiveness of tropical cyclones over the past 30 years, *Nature*, *436*, 686–688.

Fairall, C., E. Bradley, J. Hare, A. Grachev, and J. Edson (2003), Bulk parameterization of air-sea fluxes: Updates and verification for the COARE algorithm, *J. Climate*, *16*(4), 323 571–591.

Festa, J. F., and D. V. Hansen (1978), Turbidity maximum in partially mixed estuaries: A two-dimensional numerical model, *Estuar. Coast. Marine Sci.*, *7*, 347–359.

Fugate, D. C., C. T. Friedrichs, and L. P. Sanford (2007), Lateral dynamics and associated transport of sediment in the upperreaches of a partially mixed estuary, Chesapeake Bay, USA, *Cont. Shelf Res.*, *27*, 679–698.

Gelfenbaum, G., and J. D. Smith (1986), Experimental evaluation of a generalized suspended-sediment transport theory, in *Shelf Sands and Sandstones, Memoir II*, edited by R. J. Knight and J. R. McClean, pp. 133–144, Canadian Society of Petroleum Geologists, Calgary.

Geyer, W. R. (1993), The importance of suppression of turbulence by stratification on the estuarine turbidity maximum, *Estuaries*, *16*, 113–125.
Geyer, W. R., P. Hill, T. Milligan, and P. Traykovski (2000), The structure of the Eel River plume during flood, *Cont. Shelf Res.*, *20*, 2067–2093.
Goldenberg, S. B., C. W. Landsea, A. M. Mestas-Nunez, and W. M. Gray (2001), The recent increase in Atlantic hurricane activity: Causes and implications, *Science*, *293*, 474–478.
Gong, W., and J. Shen (2009), Response of sediment dynamics in the York River estuary, U.S.A. to tropical cycle Isabel of 2003, *Estuar. Coast. Shelf Sci.*, *84*, 61–74.
Gross, M. G., M. Karweit, W. B. Cronin, and J. R. Schubel (1978), Suspended sediment discharge of the Susquehanna River to Northern Chesapeake Bay, 1966 to 1976, *Estuaries*, *1*(2), 106–110.
Haidvogel, D. B., H. G. Arango, K. Hedstrom, A. Beckmann, P. Malanotte-Rizzoli, and A. F. Shchepetkin (2000), Model evaluation experiments in the North Atlantic Basin: Simulations in nonlinear terrain-following coordinates, *Dynam. Atmos. Oceans*, *32*(3-4), 239–281.
Harding, L. W., M. E. Mallonee, and E. S. Perry (2002), Toward a predictive understanding of primary productivity in a temperate, partially stratified estuary, *Estuar. Coast. Shelf Sci.*, *55*, 437–463.
Harris, C. K., P. A. Traykovski, and W. R. Geyer (2005), Flood dispersal and deposition by near-bed gravitational sediment flows and oceanographic transport: A numerical modeling study of the Eel River shelf, northern California, *J. Geophys. Res.*, *110*, 343, C09025, doi:10.1029/2004JC002727.
Harris, C. K., C. R. Sherwood, R. P. Signell, A. J. Bever, and J. C. Warner (2008), Sediment dispersal in the northwestern Adriatic Sea, *J. Geophys. Res.*, *113*, C11S03, doi:10.1029/2006JC003868.
Hill, P. S., T. G. Milligan, and W. R. Geyer (2000), Controls on effective settling velocity of suspended sediment in the Eel River flood plume, *Cont. Shelf Res.*, *20*, 2095–2111.
Jay, D. A., and J. D. Musiak (1994), Particle trapping in estuarine tidal flows, *J. Geophys. Res.*, *99*, 20,445–20,461.
Jia, P., and M. Li (2012), Circulation dynamics and salt budget in a lagoonal estuary, *J. Geophys. Res.*, *117*, C01003, doi:10.1029/2011JC007124.
Kerwin, J. A., R. E. Munro, and W. W. A. Peterson (1976), Distribution and abundance of aquatic vegetation in the upper Chesapeake Bay, 1971–1974, in the effects of tropical storm Agnes on the Chesapeake estuarine system, CRC publication No. 54, edited by E. P. Ruzecki et al., pp 393–400, The Johns Hopkins University Press, Baltimore and London.
Lerczak, J. A., W. R. Geyer, and R. J. Chant (2006), Mechanisms driving the time-dependent salt flux in a partially stratified estuary, *J. Phys. Oceanogr.*, *36*, 2296–2311.
Levitus, S. (1982), Climatological atlas of the world ocean, United States Government Printing, 354.
Li, M., L. Zhong, and W. C. Boicourt (2005), Simulations of Chesapeake Bay estuary: Sensitivity to turbulence mixing parameterizations and comparison with observations, *J. Geophys. Res.*, *110*, C12004.
Li, M., L. Zhong, W. C. Boicourt, and D.-L. Zhang (2006), Hurricane-induced storm surges, currents and destratification in a semi-enclosed bay, *Geophys. Res. Lett.*, *33*, L02604.
Li, Y., and M. Li (2011), Effects of winds on stratification and circulation in a partially mixed estuary, *J. Geophys. Res.*, *116*, C1202, doi:10.1029/2010JC006893.
Loftus, M. E., and H. H. Seliger (1976), A comparative study of primary production and standing crops of phytoplankton, in a portion of the upper Chesapeake Bay subsequent to tropical storm Agnes, in the effects of tropical storm Agnes on the Chesapeake estuarine system, CRC publication No. 54, edited by E. P. Ruzecki et al., pp 509–521, The Johns Hopkins University Press, Baltimore and London.
Lynch, M. P. (2005), An unprecedented scientific community response to an unprecedented event: Tropical storm Agnes and the Chesapeake Bay, in Hurricane Isabel in perspective, CRC publication 05-160, edited by K. G. Sellner, pp. 29–35, Chesapeake Research Consortium, Edgewater, MD.
Marchesiello, P., J. C. McWilliams, and A. Shchepetkin (2001), Open boundary conditions for long-term integration of regional oceanic models, *Ocean Modell.*, *3*(1-2), 1–20.
Mesinger, F., G. Dimego, E. Kalnay, K. Mitchell, P. C. Shafran, W. Ebisuzaki, D. Jovic, J. Woollen, E. Rogers, and E. H. Berbery (2006), North American regional reanalysis, *Bull. Am. Meteorol. Soc.*, *87*(3), 342–360.
Meade, R. H. (1982), Sources, sinks and storage of river sediment in the Atlantic drainage of the United States, *J. Geol.*, *90*, 235–252.
Mullenbach, B. L., and C. A. Nittrouer (2000), Rapid deposition of fluvial sediment in the Eel Canyon, northern California, *Cont. Shelf Res.*, *20*, 2191–2212.
North, E. W., S.-Y. Chao, L. P. Sanford, and R. R. Hood (2004), The influence of wind and river pulses on an estuarine turbidity maximum: Numerical studies and field observations in Chesapeake Bay, *Estuaries*, *27*, 132–146.
Ogston, A. S., D. A. Cacchione, R. W. Sternberg, and G. C. Kineke (2000), Observations of storm and river flood-driven sediment transport on the northern California continental shelf, *Cont. Shelf Res.*, *20*, 2141–2162.
Page, L. V., and L. C. Shaw (1973), Floods of June 1972 in the Harrisburg area, Pennsylvania, U.S. Geological Survey, Hydrologic Investigations Atlas, HA 530.
Partheniades, E. (1992), Estuarine Sediment Dynamics and Shoaling Processes, in *Handbook of Coastal and Ocean Engineering*, Vol. 3, edited by J. Herbick, pp. 985–1071, Gulf Professional Publishing, Houston, Texas.
Postma, H. (1967), Sediment transport and sedimentation in the estuarine environment, in *Estuaries*, edited by G. H. Lauff, pp. 158–179, American Associateion for the Advancement of Science, Washington, D. C.
Sanford, L. P., W. Panageotou, and J. P. Halka (1991), Tidal resuspension of sediments in northern Chesapeake Bay, *Marine Geol.*, *97*, 87–103.
Sanford, L. P., S. E. Suttles, and J. P. Halka (2001), Reconsidering the physics of the Chesapeake Bay estuarine turbidity maximum, *Estuaries Coasts*, *24*, 655–669.
Sanford, L. P., and J. P.-Y. Maa (2001), A unified erosion formulation for fine sediments, *Marine Geol.*, *179*, 9–23.
Sanford, L. P. (2006), Uncertainties in sediment erodibility estimates due to a lack of standards for experimental protocols and data interpretation, *Integr. Environ. Assess. Manag.*, *2*, 29–34.
Sanford, L. P. (2008), Modeling a dynamically varying mixing sediment bed with erosion, deposition, bioturbation, consolidation, and armoring, *Comput. Geosci.*, *34*, 1263–1283.
Schubel, J. R. (1968), Turbidity maximum of the northern Chesapeake Bay, *Science*, *161*, 1013.
Schubel, J. R. (1977), Effects of Agnes on the suspended sediment of the Chesapeake Bay and contiguous shelf waters, in *The Effects of Tropical Storm Agnes on the Chesapeake Bay Estuarine System*, edited by J. Davis and B. Laird, pp. 179–200, Johns Hopkins Univ. Press, Baltimore.
Schubel, J. R., and H. H. Carter (1977), Suspended sediment budget for Chesapeake Bay, in *Estuarine Processes*, edited by M. L. Wiley, pp. 48–62, Academic Press, New York.
Schubel, J. R., and C. F. Zabawa (1977), Agnes in the geological record of the upper Chesapeake Bay, in *The Effects of Tropical Storm Agnes on the Chesapeake Bay Estuarine System*, edited by J. Davis and B. Laird, pp. 240–248, Johns Hopkins Univ. Press, Baltimore.
Smullen, J. T., J. Taft, and J. Macknis (1982), Nutrient and sediment loads to the tidal Chesapeake Bay system, in *Chesapeake Bay Program Technical Studies: A synthesis*, edited by E. G. Macalaster, D. A. Barker and M. Kasper, pp 147–262, U.S. Environment Protection Agency, Washington, DC.
Sommerfield, C. K., and C. A. Nittrouer (1999), Modern accumulation rates and a sediment budget for the Eel shelf: A flood-dominated depositional environment, *Marine Geol.*, *154*, 227–241.
Traykovski, P., W. R. Geyer, J. D. Irish, and J. F. Lynch (2000), The role of wave-induced density-driven fluid mud flows for cross-shelf transport on the Eel River continental shelf, *Cont. Shelf. Res.*, *20*, 2113–2140.
Wang, P., and L. C. Linker (2005), Effect of timing of extreme storms on Chesapeake Bay submerged aquatic vegetation, in Hurricane Isabel, in *perspective, CRC publication 05-160*, edited by K. G. Sellner, pp. 177–184, Chesapeake Research Consortium, Edgewater, MD.
Warner, J. C., W. R. Geyer, and J. A. Lerczak (2005), Numerical modeling of an estuary: A comprehensive skill assessment, *J. Geophys. Res.*, *110*, C05001, doi:10.1029/2004JC002691.
Warner, J. C., C. R. Sherwood, R. P. Signell, C. K. Harris, and H. G. Arango (2008), Development of a three-dimensional, regional, coupled wave, current, and sediment-transport model, *Comput. Geosci.*, *34*, 1284–1306.
Webster, P. J., Holland G. J., J. A. Curry, and H.-R. Chang (2005), Changes in tropical cyclone number, duration, and intensity in a warming environment, *Science*, *309*, 1844.
Wheatcroft, R. A. (2000), Oceanic flood sedimentation: A new perspective, *Cont. Shelf Res.*, *20*, 2059–2066.
Wheatcroft, R. A., and J. C. Borgeld (2000), Oceanic flood deposits on the northern California shelf: Large-scale distribution and small-scale physical properties, *Cont. Shelf Res.*, *20*, 2163–2190.
Wright, L. D., C. T. Friedrichs, S. C. Kim, and M. E. Scully (2001), Effects of ambient currents and waves on gravity-driven sediment transport on continental shelves, *Marine Geol.*, *175*, 25–45.
Xu, J., R. R. Hood, and S.-Y. Chao (2005), A simple empirical optical model for simulating light attenuation variability in a partially mixed estuary, *Estuaries Coasts*, *28*, 572–580.
Xu, K., C. K. Harris, R. D. Hetland, and J. M. Kaihatu (2011), Dispersal of Mississippi and Atchafalaya sediment on the Texas-Louisiana shelf: Model estimates for the year 1993, *Cont. Shelf Res.*, *31*, 1558–1575.
Zhong, L., and M. Li (2006), Tidal energy fluxes and dissipation in the Chesapeake Bay, *Cont. Shelf. Res.*, *26*, 752–770.